Journal of South American Earth Sciences 26 (2008) 271–285

Contents lists available at ScienceDirect

Journal of South American Earth Sciences

journal homepage: www.elsevier.com/locate/jsames

Geophysical evidence of crustal-heterogeneity control of fault growth in the Neocomian Iguatu basin, NE Brazil

David L. de Castro [a,*], Francisco H.R. Bezerra [b], Raimundo M.G. Castelo Branco [a]

[a] Laboratório de Geofísica de Prospecção e Sensoriamento Remoto – LGPSR, Departamento de Geologia, Universidade Federal do Ceará, Campus Universitário do Pici, Bloco 913, 60455-760 Fortaleza – CE, Brazil
[b] Departamento de Geologia, Universidade Federal do Rio Grande do Norte, Campus Universitário, Lagoa Nova, 59.078-970 Natal – RN, Brazil

ARTICLE INFO

Article history:
Received 11 July 2007
Accepted 28 July 2008

Keywords:
Airborne geophysics
Gravity modeling
Rift evolution
Crustal reactivation
Iguatu basin
NE Brazil

ABSTRACT

Models of fault growth propose that rift initiation starts with short fault segments. Knowledge of the growth of these segments and their interactions is important to understanding rift geometry and evolution. In the northern part of the Borborema Province, northeastern Brazil, a continental-scale, Cretaceous extensional system of faults has been observed to have reactivated ductile Precambrian shear zones. The faults form small grabens that represent the rift stage of the sedimentary basins. We integrated airborne radiometric and magnetic data with terrestrial gravity survey to investigate the influence of crustal heterogeneity on fault growth and the development of the extensional faults in one of these grabens, the Iguatu basin. Previous studies presented geophysical data, which provide evidence that the Iguatu basin contains a half-graben geometry. In our study, gravity and airborne geophysical data indicate that the basement of the Iguatu basin is part of a heterogeneous structural framework composed of two structural domains, is affected by several ductile shear zones and intruded by a few granite bodies. The gravity modeling reveals that this basin is composed of three right-bend en echelon fault segments. They form a sigmoid system of normal faults that accommodate the strong ~90° bend of the Precambrian shear zones from E–W to roughly N–S. The growth of these segments led to the generation of two isolated depocenters. The overlapping fault segments link through relay ramps. Release faults that are nearly perpendicular or oblique to the three main fault segments form marginal strike ramps and horst structures in both depocenters. 3D-gravity modeling incorporates the presence of interfering sources of a heterogeneous structural framework. The modeling reveals a maximum sedimentary cover 1620 m thick, which occurs at the bend of the reactivated shear zones. The gravity signature of a possible granite body, after removal of the gravity effect of the basin-filling deposits, indicates that this possible intrusion forms a horst oriented roughly parallel to the basement fabric. The relationship between maximum displacement and fault length indicates that the fault segments formed independently during the initiation of the half-graben. But the fault segments, linked by relay ramps, influence the development of one another. We interpret the segments to represent a pre-linkage, multisegmented stage of an aborted rift system. This pattern of fault growth may have also influenced the rift stage of other sedimentary basins in the region.

1. Introduction

Investigating fault growth requires understanding how fault segments evolve into a single linked fault. Current theoretical and experimental models of fault growth have been tested using observational evidence from the earliest stages of rift development. These models have been based on detailed field observations (e.g., Dawers et al., 1993) and on seismic data (e.g., Pickering et al., 1997). These studies have also shed light on the influence of crustal heterogeneity and preexisting structural fabric in the evolution of rift basins (e.g., Cartwright et al., 1995; Cowie et al., 2000; McLeod et al., 2000).

Poor field exposure of exhumed rifts, lack of data on basement fabric, and seismic data that do not cover the whole fault system, especially its tips, are problems to be overcome in the development of fault-growth models. Problems with existing fault-growth models point to the need for further work on case studies, especially to relate the slip events to finite displacement of faults and to link detailed field observations with realistic models (e.g., Peacock, 2002). In this sense, the structural framework of a rift system can be better constrained by detailed geophysical surveys where lithotypes of the rift phase are exposed or partially buried and where magnetic and gravity interference caused by post-rift sedimentary covers are absent or irrelevant.

* Corresponding author. Fax: +55 2185 3366 9870.
E-mail addresses: david@ufc.br (D.L. de Castro), bezerrafh@geologia.ufrn.br (F.H.R. Bezerra).

0895-9811/$ - see front matter © 2008 Elsevier Ltd. All rights reserved.
doi:10.1016/j.jsames.2008.07.002

The Cretaceous Iguatu basin in northeastern Brazil contains characteristics that allow investigation of fault growth in an early rift stage. The basin forms a small graben of Neocomian age that crops out and can be directly investigated to reveal the relationship between basement fabric and fault growth. The absence of post-rift sedimentary rocks contributed to the investigation.

The main aim of this paper is to combine gravity and airborne radiometric–magnetic data to assess how basement fabrics control fault growth and rift architecture in the Neocomian Iguatu basin. We describe the 3D complexities of the basin and extrapolated the results for other basins in the region, where the rift phase is buried by post-rift units. We hope that our study can contribute to understanding the early evolution of faults during crustal extension and rifting, as well as the tectonic evolution of the Cretaceous system of rifts in northeastern Brazil.

2. Tectonic setting and geology of the Iguatu basin

The Iguatu basin is inserted in the Precambrian basement grain, named Borborema Province (Fig. 1). In a broader sense, the Borborema Province is a shield that consists of Archean to Proterozoic inliers amalgamated along volcano-sedimentary belts (e.g., Neves et al., 2000). A pervasive low-angle foliation and a network of steep, continental-scale, strike-slip ductile shear zones, mostly formed during the Brasiliano–Pan African orogenic cycle (0.8–0.5 Ga), affect this province. During that period, syn- to late-kinematic granite bodies intruded the Borborema Province (Almeida et al., 2000).

The shear zones form a network of sigmoid NE- and E–W-trending features (Fig. 1) that are dozens to hundreds of kilometers long and a few kilometers wide. Most of these zones reactivated in a

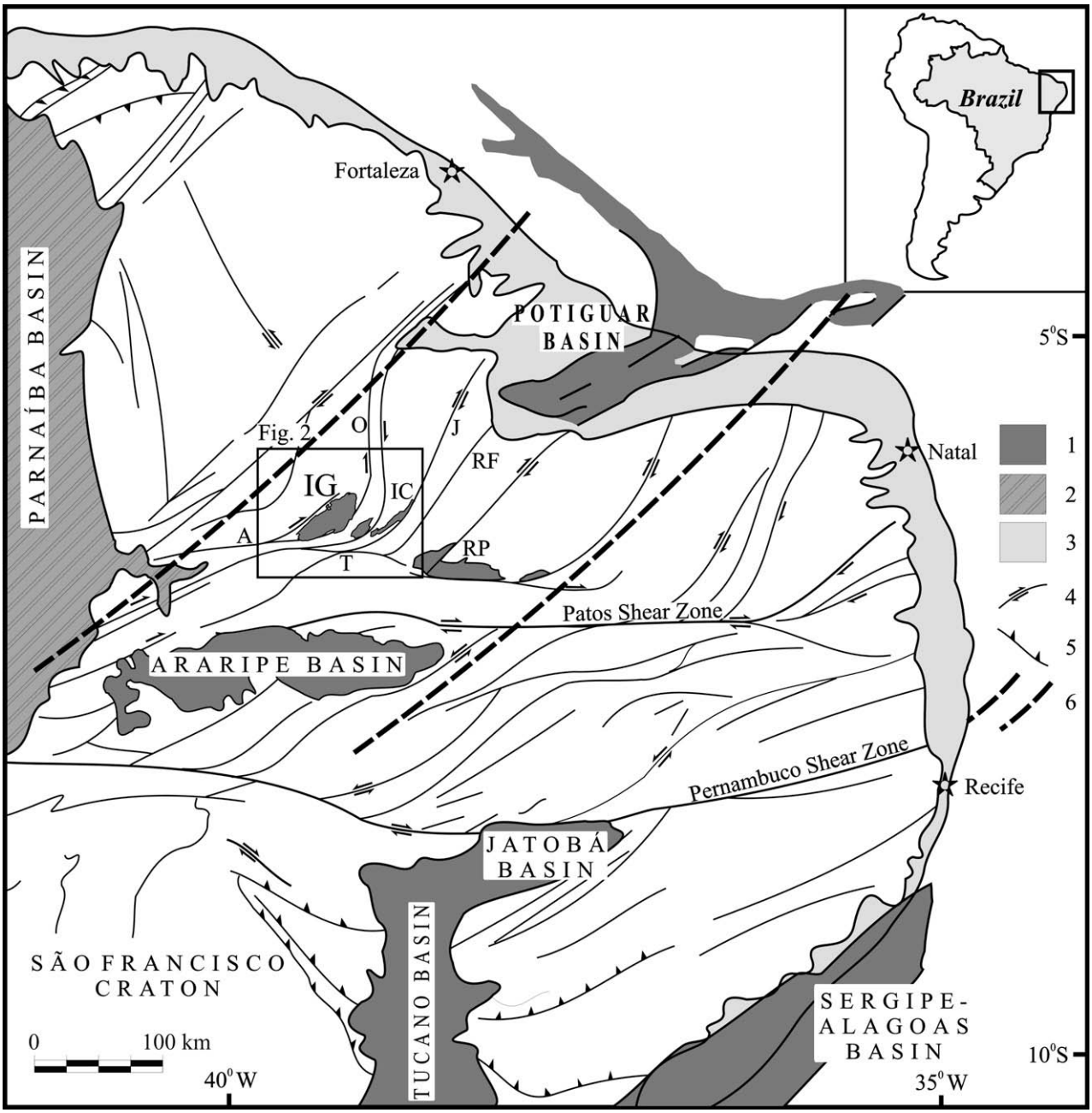

Fig. 1. Simplified geological map of the Borborema Province, showing the distribution of sedimentary basins and major geologic features: 1, Cretaceous Cariri Valley rift basins (IC – Icó, IG – Iguatu, RP – Rio do Peixe); 2, Paleozoic sedimentary rocks of the Parnaíba basin; 3, Coastal Cretaceous–Cenozoic sedimentary cover; 4, strike-slip shear zones (A –Aiatuba, J – Jaguaribe, O – Orós, RF – Rodolfo Fernandes, T – Tatajuba); 5, thrust shear zones; and 6, Cariri–Potiguar Trend.

brittle regime in the early Cretaceous during the onset of the Pangea breakup. The main extension took place along a NW–SE-trending axis as indicated by surface-geology and deep seismic-reflection investigations (Matos, 1992). It led to localized crustal thinning below the Cariri–Potiguar trend (Castro et al., 1998). According to Matos (1992), the Cariri–Potiguar trend encompasses one of three major rift valleys of the Northeast Brazilian Rift System. A series of NE-trending intracratonic basins have been formed along this trend, including the Iguatu basin.

Reactivation of the shear zones during the Neocomian led to the formation of the basins separated by structural and topographic highs. The most important basins are the Iguatu, Malhada Vermelha, Lima Campos, Icó, and Rio do Peixe (Fig. 2), which correspond to half-grabens with steep NW-dipping master faults located on their southeastern edges.

The Precambrian tectonostratigraphic setting in which the Iguatu basin occurs encompasses two lithostructural domains north of the Patos shear zone (Figs. 1 and 2). Both domains consist of lithostructural associations that include orthogneisses and metasedimentary sequences, intruded by Neoproterozoic granites, and cut across by dextral shear zones (Cavalcante, 1999). The Orós–Jaguaribe domain encompasses two roughly parallel NNE-trending linear belts (Arthaud et al., 2000), which bend and reach an E–W direction in the southern part of the domain. The belts are made of Late Paleoproterozoic metasedimentary and metavolcanic rocks, intruded by Late Paleoproterozoic granites, and consist of high- to medium-grade metamorphic terrains 370 km long, with steep dipping foliation and sub-horizontal stretching lineation (Sá et al., 1995). A good example is the West-Orós and East-Orós shear zones, which mark the geologic contact between Orós and Jaguaribe sub-domains. In the southern boundary of the Iguatu basin, metavolcanic and metasedimentary sequences form the Granjeiro domain, which was affected by the Brasiliano Cycle, resulting in a NE–SW to E–W-trending recumbent structure.

The Iguatu basin was filled during two tectonic-depositional pulses in the Early Cretaceous by syn-rift alluvial, fluvial, and lacustrine deposits (Bedregal, 1991; Ponte Filho, 1996). The first pulse corresponds to the Rio da Serra stage and encompasses the Icó and Malhada Vermelha formations, which consist of basal conglomerates and coarse-grained sandstones, overlain by sandstones, siltstones, and mudstones. They deposited in a fluviatile to lacustrine environment. The second tectonic-depositional pulse formed the Lima Campos Formation during the Aratu Stage. This upper formation is composed of sandstones interbedded with mudstones and shale lenses. They deposited on floodplains and fluvial fans, or within shallow lakes (Ponte Filho, 1996).

Magmatic activity occurred in the Late Jurassic to the north of the Iguatu basin. It formed a swarm of mafic dikes, which intruded the Precambrian basement with a main ENE–WSW trend (Matos, 1992). This dike swarm, named Rio Ceará Mirim Magmatism by Gomes (1981), occurred in two main pulses at 145 and 130 Ma (Oliveira and Chang, 1993), and represents the last activities that preceded the onset of the syn-rift phase in the Cariri–Potiguar Trend.

3. Methods

3.1. Dataset and processing of airborne geophysical data

We used an aerogeophysical survey, named Iguatu Project, carried out in the northern part of Borborema Province between 1976 and 1977 by the Brazilian Geological Survey (CPRM). The project covered a 52,000 km^2 area with gamma-ray spectrometry and magnetometry, which yielded a 55,000 km line of surveyed data. The Iguatu basin lies at the middle part of the Iguatu Project. CPRM

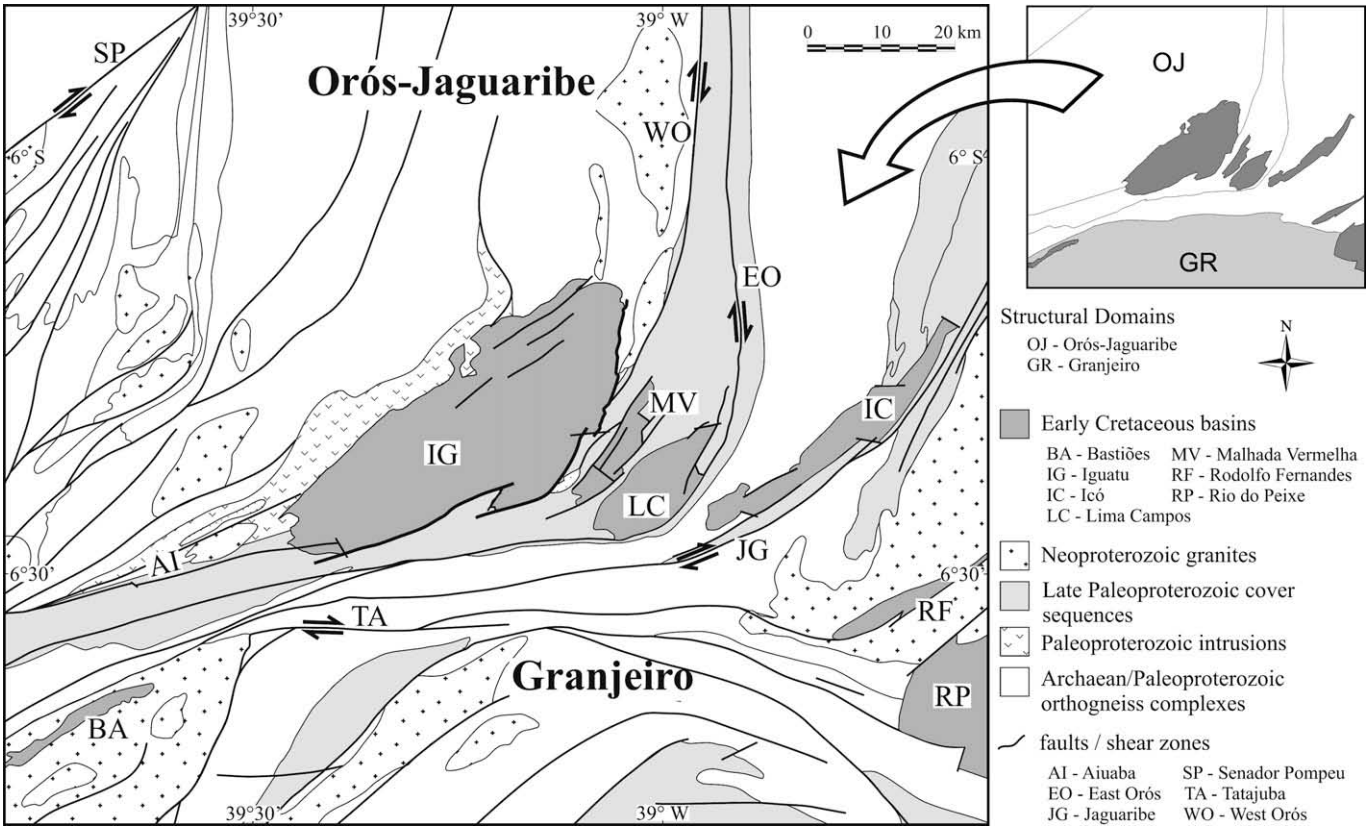

Fig. 2. Simplified geologic map of the Iguatu basin area (modified from Vasconcelos and Gomes, 1998).

collected the data on N45°E-oriented flight lines, with 1.0 km spacing, sample rate of 100 m, and nominal flight height of 150 m above the ground. CPRM also carried out the necessary corrections related to the survey data, including the variable altitude and the International Geomagnetic Reference Field (IGRF) (MME/CPRM, 1995).

We interpolated the airborne geophysical data using the Kriging method with 0.5 km regular spacing. The variogram model parameters used for kriging were defined based on the semi-variogram of the geophysical data. The statistical accuracy of kriged results has been analyzed through the RMS difference between the variogram models and the observed variogram. We then filtered magnetic and radioelement abundance of K, Th, U, and total-count maps to eliminate high-frequency noise related to the high sample rate along flight lines. The filter we selected works in the frequency domain as a general directional cosine filter and rejects trends in a specified azimuth direction (Cordell et al., 1992). The cosine function makes the filter smooth. Therefore, directional ringing problems are usually not a problem. The direction of the filter had the same N45°E-oriented direction of the flight lines. The degree of the cosine function was chosen to remove the directional noise without, however, attenuating the signal content in that specific direction. As a result, the filter attenuated high-frequency directional noise.

Magnetic anomalies were also reduced to the pole (RTP) to remove the distortion caused by the geomagnetic field and to produce maxima over magnetic contacts, regardless of the distribution of magnetization. This means that the magnetic anomalies can be viewed in map form with a vertical magnetic field inclination and zero declination. In this way, the interpretation of the data was made easier as vertical bodies would produce magnetic anomalies centered on the symmetric body. However, when reducing to the pole from equatorial latitudes, N–S features can blow up due to the strong amplitude correction that is applied when geomagnetic declination is $\pi/2$ (i.e. a magnetic E–W wavenumber). By specifying a higher latitude for the amplitude correction alone, this problem can be reduced or eliminated at the expense of undercorrecting the amplitudes of N–S features. The parameters of the geomagnetic field used in RTP had an inclination of $-5.75°$ and declination of $-20.7°$. An inclination of 80° for amplitude correction yielded magnetic anomalies reduced to pole, which are free of instabilities. These instabilities are commonly associated with reduction to the pole of low-latitude data.

In addition, we obtained the amplitude of the three-dimensional analytic signal of the magnetic field to improve the delineation of the magnetic lineaments in the Iguatu dataset. This technique, initially performed by Nabighian (1984), produces maxima over magnetic sources irrespective of their magnetization direction. In the technique, the 3D analytic signal is the square root of the sum of the squares of the derivatives in the *x*-, *y*-, and *z*-directions. We obtained the horizontal derivatives with a spline interpolator and computed the vertical gradient using the Fourier transforms.

3.2. Dataset and 3D modeling of gravity data

We carried out a gravity survey in the Iguatu-basin area. The survey yielded 462 gravity stations, which, combined with gravity-observation points from previous surveys (Bedregal, 1991;

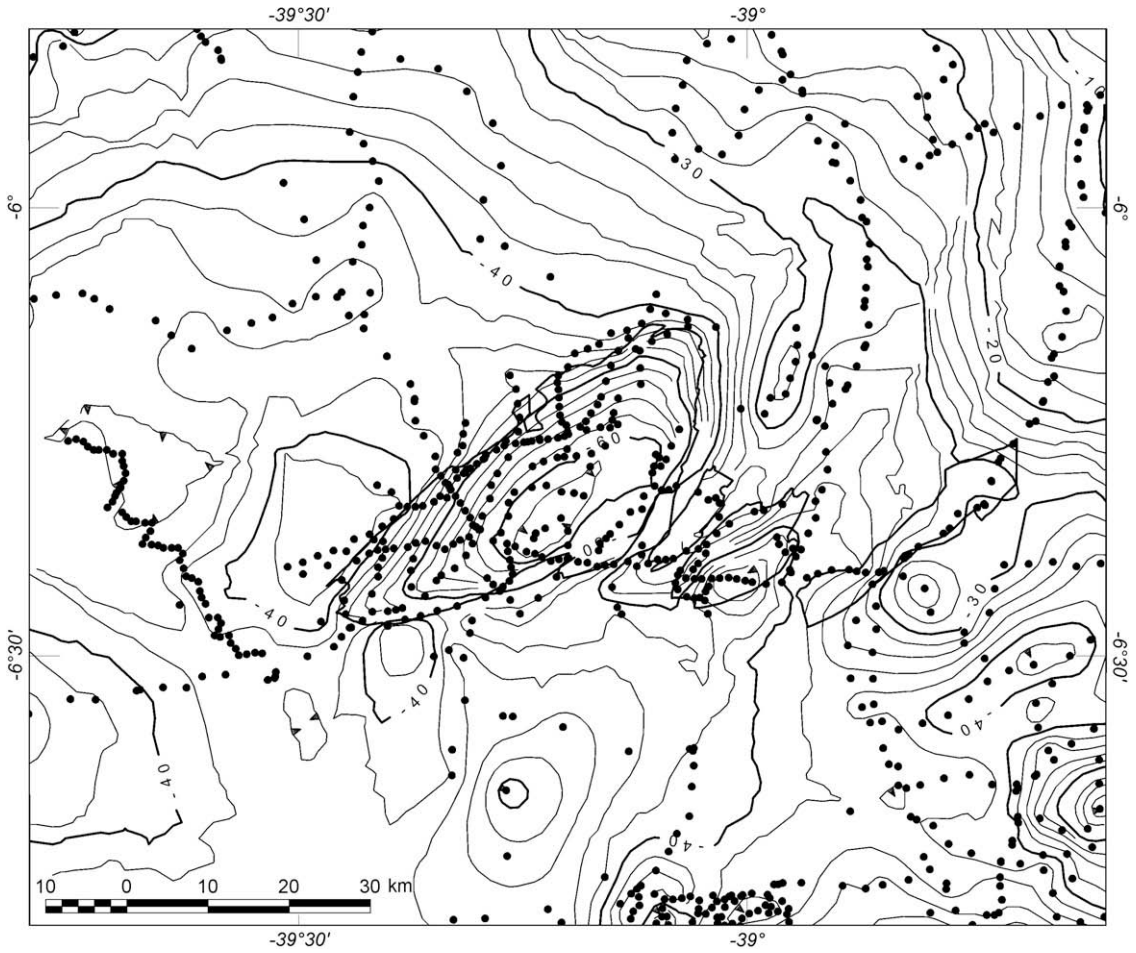

Fig. 3. Bouguer anomaly map of the Iguatu basin and location of gravity stations.

Castro et al., 1998; Castro and Castelo Branco, 1999), comprise a dataset of 737 measurements (Fig. 3). In each station, we used a Lacoste-Romberg Model G gravity meter, with ±0.01 mGal precision. We determined geographic coordinates and elevation using both differential GPS and barometer arrays. We also applied drift, latitude, free-air, and Bouguer reductions, referring the data to the international system of gravity IGSN-71. Finally, we interpolated the gravity maps at 15,008 equally spaced points with 1.0 km station interval. The scarcity of data in some locations yields an indirect smoothing effect on the final gravity map. The influence of this effect, however, is attenuated in the Iguatu basin area, where, on average, each gravity station covers a 4 km^2 area.

We applied a regional–residual separation filter to the Iguatu basin and the adjoining basement rocks because the residual gravity data tend to reflect shallow density distributions. Afterwards, we estimated the residual gravity field by applying a Gaussian regional/residual filter with 0.8 cycles/km cut-off frequency.

We constructed a 3D model of the gravity anomaly using the algorithm developed by Castro (2005). This algorithm simulates gravity anomalies of a group of vertical rectangular prisms in the observed field. The method is similar to the one developed by Jachens and Moring (1990). The algorithm departs from other methods by taking into account the possibility that basement rocks that underlie sedimentary basins have variable density. It strives to separate gravity measurements into the component caused by the basin itself and the component resulting from variations in density of the underlying basement, as described in detail by Blakely (1995).

We also used the new residual data to find a first approximation to basement depth using the iterative procedure developed by Rao and Babu (1991). This method determines the shape, at depth, of an interface that separates two homogeneous media. In the method, a quadratic function accounts for an increase in density with depth within the basin due to the compaction of sediments. This function is represented by $[\Delta\rho(z) = a_0 + a_1 z + a_2 z^2]$, where z represents the depth; a_0, the extrapolated value of density contrast at the surface in g/cm^3; and a_1 and a_2, the constants of the function.

We finally calculated the gravitational effect of the basin and subtracted it from basement gravity stations to produce the next approximation for the pattern of basement gravity. We repeated this procedure until the solution converged to a satisfactory separation of basin and basement gravity. We obtained the shape of the low-density basin and the gravity field of the basement, without the effects of the basin.

The calculated thickness of basin-filling deposits depends critically on the density–depth function used in the modeling (Blakely et al., 1999). In our study, we carried out 48 density measurements on selected samples that represented sedimentary and basement rocks. We established the medium-density contrast in surface to be -0.642 ± 0.05 g/cm^3. This superficial contrast, however, does not reflect the density increase of the sedimentary deposits with depth. We opted to use the density vs. depth data from the Potiguar basin to achieve a more realistic density–depth distribution for the inversion of the Iguatu-basin dataset. The reason for this option was that the petrophysical parameters of the Potiguar basin are known as a result of intensive oil exploration since the 1970s (e.g., Mello, 1989) and because the early infill of this basin is similar to that of the Iguatu basin. We fitted the dependence of the sediment density with depth to a quadratic function by the least-square method, extracted from well-logging data from the Potiguar basin (Castro et al., 2007). Eventually, we estimated the coefficients of the function as follows: $a_0 = -0.297$ g/cm^3, $a_1 = 7.097 \times 10^{-5}$ g/cm^3, and $a_2 = -8.836 \times 10^{-11}$ g/cm^3. Castro et al. (2007) obtained a difference of 7.4% when they compared the 3D-gravity modeling of the Rio do Peixe basin (Fig. 1) with a stratigraphic well. If this variation is extrapolated to the Iguatu basin, we can assume that the inverse method exhibits good confidence.

4. Geophysical features of the Iguatu basin

4.1. Radiometric signature

The superficial distribution of total counts enabled us to identify the major geological features at the Iguatu basin from the analyzed radioelement abundance of K, Th, U, and total count (Fig. 4). The total-count signature reveals a complex distribution of various radiometric units, whose geological context comprises Archean and Paleoproterozoic orthogneiss complexes, Proterozoic volcano-sedimentary belts, and pre to syn-Brasiliano granite intrusions.

We identified eight radiometric units characterized by high radioelement counts (600–2500 cps). The units represent Archean to early Proterozoic orthogneiss complexes and a few granite intrusions. The orthogneiss complexes occur in both domains, whereas the intrusions that show high counts concentrate south of the Tatajuba shear zone in the Granjeiro domain.

In contrast, eight low-radiometric units (less than 600 cps) represent Neoproterozoic volcano-sedimentary belts, pre-Brasiliano and Brasiliano plutonic rocks, and sedimentary basins. The major low-radiometric unit is located between West-Orós and East-Orós shear zones and encompasses metasedimentary sequences of the Orós Group, as well as Paleoproterozoic deformed granite bodies and sedimentary rocks. The radiometric signature of the Iguatu basin consists of low total-count values (>100 cps). Normally, the radioelement counts increase up to 850 cps, but few maxima show values higher than 1150 cps in the western part of the basin. These are typical counts of terrigenous infill of sedimentary basins.

The major E–W- to NE–SW-trending shear zones form sigmoid-shaped positive total-count anomalies. In the central part of the study area, radiometric lineaments reveal a principal trend between N40° and N70°E. In the southern part, the major lineament directions concentrate around N75°E. At the Iguatu basin, in the central part of the study area, radiometric alignments are NE–SW-oriented and parallel to the major pre-rifting structures of the Archean and Paleoproterozoic orthogneiss complexes.

4.2. Magnetic signature

The magnetic anomaly map reduced to the pole (Fig. 5A) shows a complex structural framework in the Iguatu-basin area. In the Orós–Jaguaribe domain, magnetic anomalies form NE–SW-trending zones of alternating polarity, whose amplitudes vary from −30 to 45 nT and from −70 to 55 nT west and east of the Orós shear zone, respectively. This magnetic pattern reflects a complex combination between lateral contrasts of magnetization and some possible contribution of remanent magnetization, which modify the anomalies of the local magnetic field to either positive or negative values. An E–W-trending, magnetic lineament occurs south of the Iguatu basin. It bends to NE–SW, where it marks the contact between the Orós–Jaguaribe and Granjeiro domains. Major shear zones form positive-magnetic anomalies with short wavelength (Figs. 2 and 5). They are partially truncated by another set of aligned anomalies, which represent diabase dikes of the Mesozoic Rio Ceará Mirim Magmatism. To the southwest, the Archean-Proterozoic Granjeiro domain produces high positive anomalies (up to 50 nT), which trend E–W and bend toward NE–SW in the east part of the study area. All those bends indicate a dextral movement along an E–W direction.

The magnetic pattern of the Iguatu basin comprises a zone of NE–SW-trending negative and positive anomalies, which show low to medium amplitude (−30 to 15 nT) and medium to high wavelength, respectively (Fig. 5A). The NE–SW-trending positive anomalies at the southeastern part of the basin probably repre-

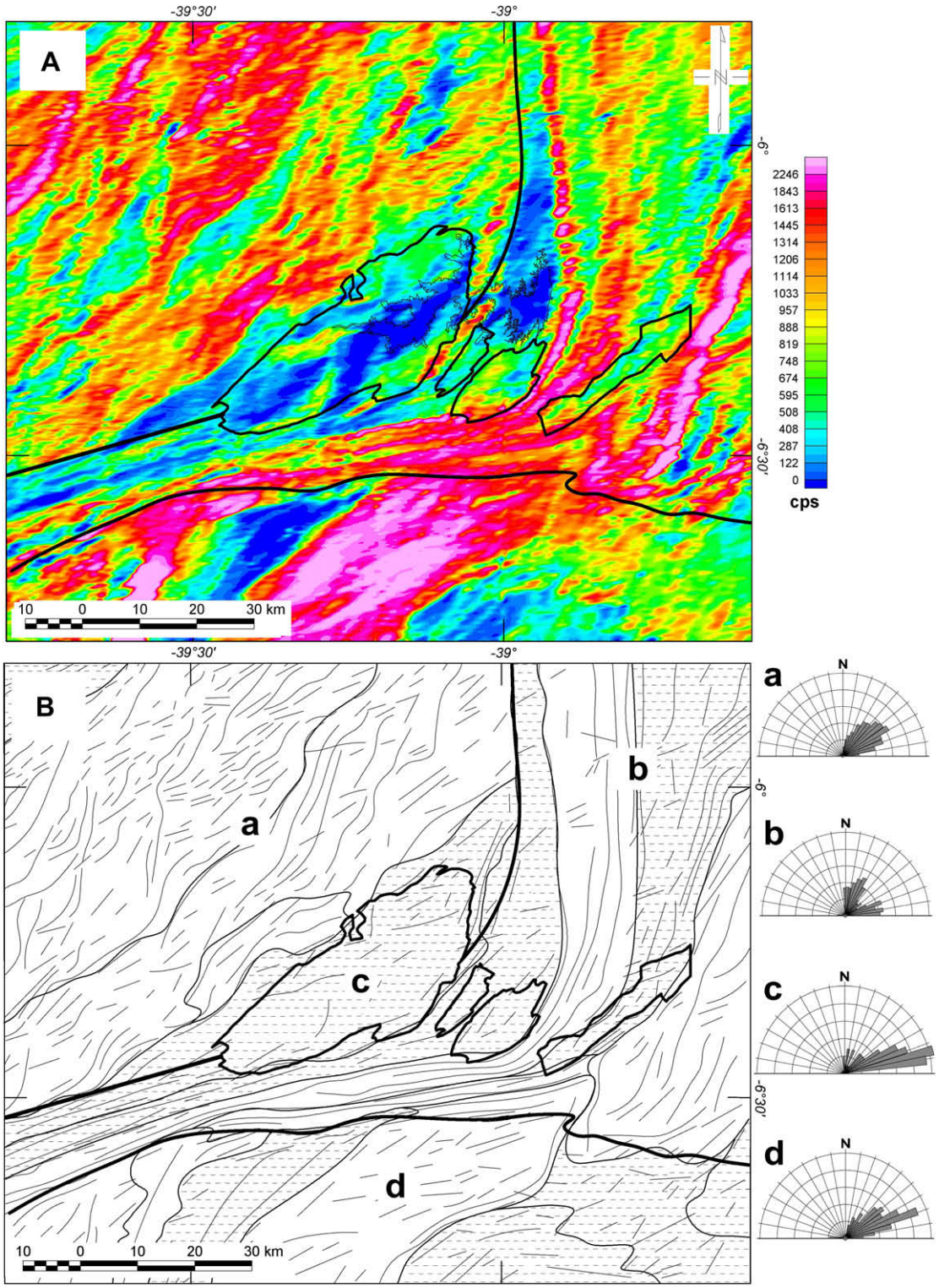

Fig. 4. (A) Gamma-ray U counts of the Iguatu basin; and (B) major radiometric domains and lineaments. Rose diagrams of lineament strike for each tectonic domain: a – Orós sub-domain; b – Jaguaribe sub-domain; c – Iguatu basin; and d – Granjeiro domain. The limits and main lineaments are indicated.

sent a horst-like feature in the basement. The anomalies seem to reflect lithologic-basement heterogeneities beneath the basin. Inside the basin, the variation in magnetic pattern reflects mainly the composition of the basement rather than the thickness of sedimentary infill; and along its northern half the anomaly in the basin is in good agreement with a positive anomaly in the adjacent basement.

The 3D analytic signal map (Fig. 5B) emphasizes the magnetic patterns. In general, high amplitudes of the analytic signal mark shear zones, whereas low amplitudes mark the Iguatu basin and non-sheared crystalline rocks in the Orós belt. This pattern is interrupted by extensive NE–SW-trending (N50°–N70°E) amplitudes maxima, which mark the western and eastern boundaries of the basin. The distribution of analytic signal shows high amplitudes

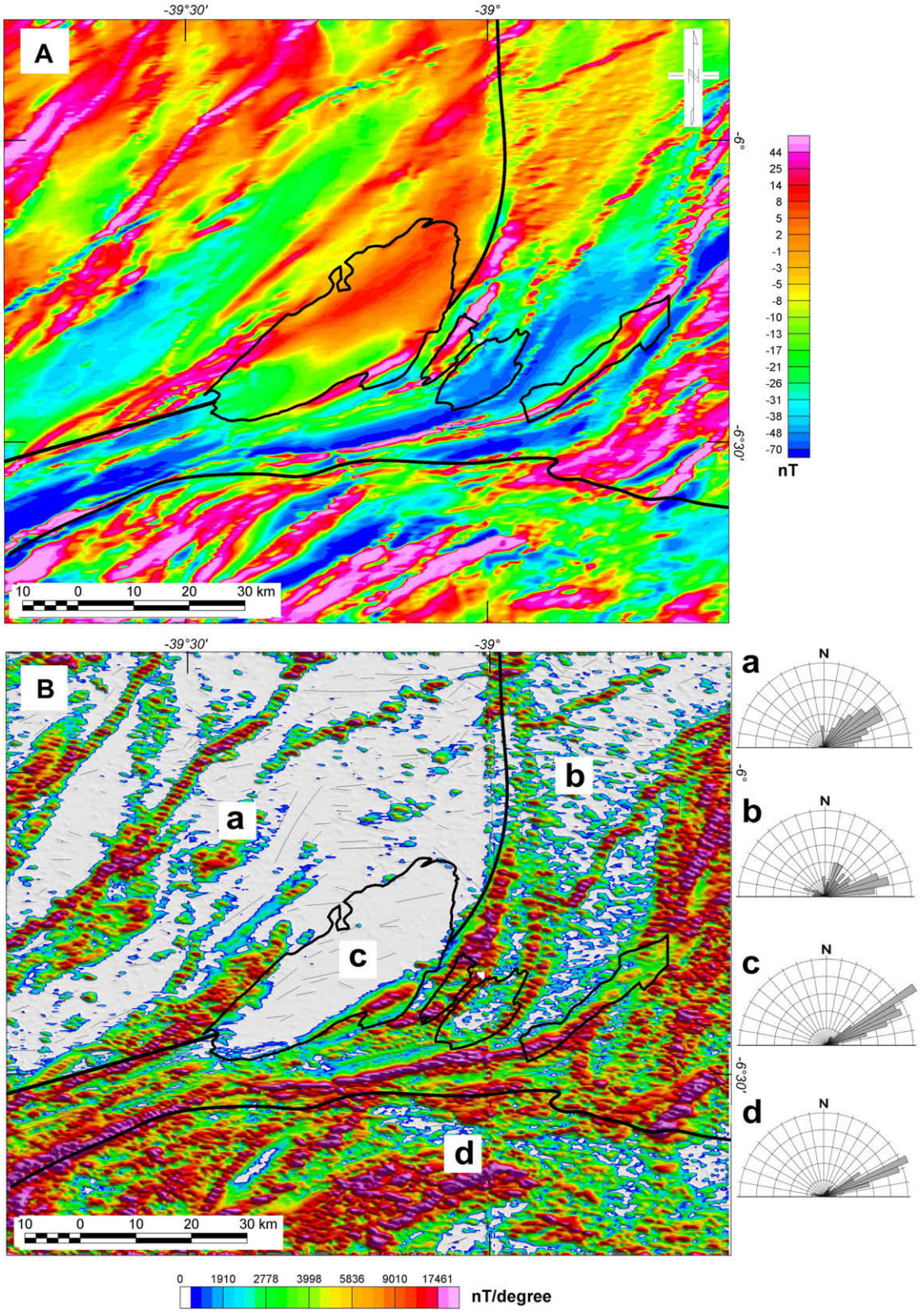

Fig. 5. (A) Magnetic anomaly map reduced to the pole; and (B) 3D analytic signal map of the Iguatu basin area. Rose diagrams of lineaments strike for each tectonic domain: a – Orós sub-domain; b – Jaguaribe sub-domain; c – Iguatu basin; and d – Granjeiro domain. The limits and main lineaments are indicated.

that form a rugged magnetic relief to the south of the Tatajuba shear zone and in the Jaguaribe belt. In these areas, the magnetic alignments show a preferential NE–SW orientation, N65°E to the south of the Tatajuba shear zone and N75°E in the Jaguaribe belt. In the northern part of the study area, the magnetic lineaments bend to NNE–SSW, following the East- and West-Orós shear zones.

4.3. Gravity signature

The residual gravity map shows contrasting gravity patterns. The Iguatu basin forms a 60 km long NE–SW-trending negative-gravity anomaly (Fig. 6A). Two minima occur along the eastern basin border, where the gravity field reaches values about −18 mGal. This pattern indicates that the Iguatu basin has a half-graben internal structure, whose deepest part occurs on its eastern side. Previous geological and geophysical studies support this interpretation (Bedregal, 1991; Ponte Filho, 1996; Castro and Castelo Branco, 1999).

Crystalline rocks contain a more complex pattern. Certainly, the poor sampling rate of gravity measurements causes an indirect smoothing effect mainly on the basement gravity signature. It is our opinion, however, that interpretations based on the gravity maps presented here are useful at the regional scale. In

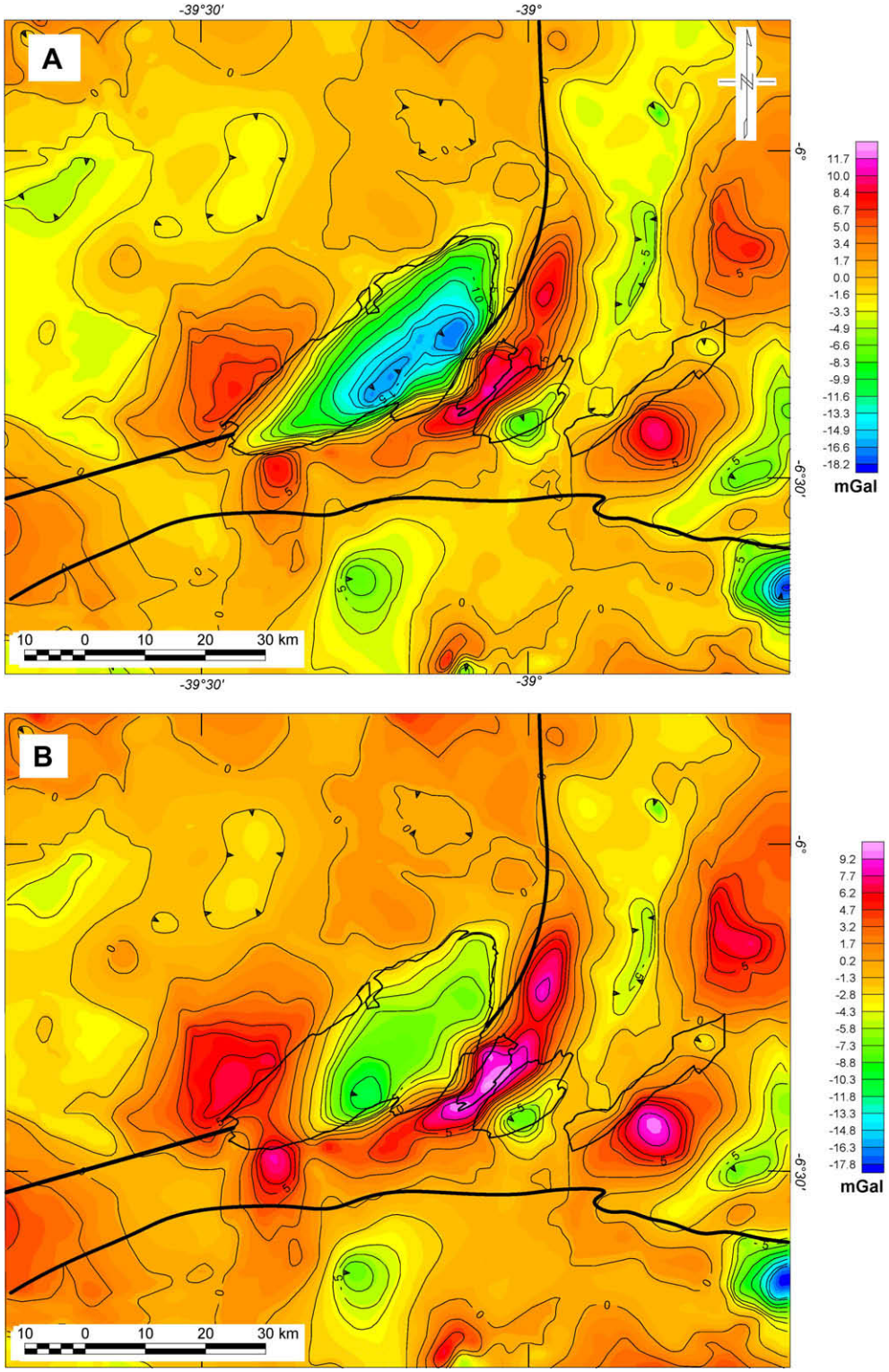

Fig. 6. (A) Residual anomaly map of study area; and (B) residual anomaly map of the basement without the gravity effect of the Iguatu basin.

general, the gravity signature of the Orós–Jaguaribe and Granjeiro domains consists of positive and negative anomalies with low amplitudes (−6 to 7 mGal) and short to medium wavelength. In the westernmost area, negative-gravity anomalies represent Paleoproterozoic rocks and granite intrusions. In the southeast part of the study area, south of the Tatajuba shear zone, a −7 mGal anomaly also represents a granite intrusion. Positive anomalies also occur at the western and southern boundary of the Iguatu basin. They mark the eastern borders of the Iguatu and Icó basins. We associate these positive anomalies with metaplutonic rocks.

Fig. 6B shows the residual anomaly map without the gravity effects of the Iguatu basin. A new anomaly of −10 mGal appears in the basin area, indicating a less dense gravity source in the basement grain. The anomaly shape roughly resembles a NE–SW-trending ellipsoid. The central area of the anomaly is dislocated from the two gravity minima observed in the residual map (Fig. 6A). A possible granite source beneath the basin could have generated this negative anomaly in this area. Similar gravity minima occur west and south of the basin in the Granjeiro domain and in the Orós sub-domain, respectively.

We modeled the negative anomaly beneath the basin to provide an estimate of the geometry of the related body. We assumed that the medium-density of a granite and its neighboring crystalline basement equaled 2.64 and 2.75 g/cm^3, respectively (Telford et al., 1998). This led to a density contrast at surface of −0.11 g/cm^3. Fig. 7 depicts the gravity model of the basin and the geometry of the body associated with the negative anomaly. The anomaly extrapolates the basin boundaries at the NE border. Estimates of the size of the related body indicate maximum depth ~4.0 km, which coincides with the location of the major horst structure of the basin. The southwestern part of the anomaly indicates an aligned N–S-trending body. In this area, the body displays a roughly sub-horizontal floor with several gently dipping areas. In contrast, the central and northeastern parts of this anomaly take the shape of a thin sheet less than 0.5 km thick, which shows a flat-basal contact with neighboring rocks. The lithologic composition of this basement high, however, remains speculative because information about boreholes or other geophysical data, such as those from electric and electromagnetic methods, is not available. Therefore, a basement high exposed at surface splits the Rio do Peixe basin into two sub-basins (Fig. 1). Castro et al. (2007) suggested that this granite body probably anchored and deviated the mechanical subsidence of that basin. A similar mechanism could have occurred in the Iguatu basin.

We determined the internal architecture of the Iguatu basin based on 3D-gravity modeling and magnetic and radiometric analyses. The basement contour map and the block diagram of Figs. 8 and 9 show the geometry of the principal types of faults and associated structures of the Iguatu basin. The geologic architecture of the basin corresponds to a half-graben made up of three master faults, which reactivated the Aiauba and West-Orós shear zones (see Fig. 2). The faults occur at the southern and eastern borders of the half-graben with an average dip of 74°NW and strikes that vary between 005° (eastern border) and 070° (southern border). A maximum displacement of 1.62 km was observed in fault segment (c), whose trace length reaches 32.7 km.

The internal geometry of the basin is associated with significant sedimentary variations in thickness. The maximum sedimentary thickness reaches 1.62 km close to the eastern border of the basin. It becomes thinner progressively to the NW-basin boundary. The basin contains two isolated depocenters separated by a 0.35 km deep intra-basin high. This high forms a horst structure, probably composed of a granite body and marked by a −10 mGal anomaly in the gravity map without the effect of the basin infill (see Fig. 6B). The northeast depocenter occurs at the intersection of the central and northern fault segments (segments (b) and (c) in Fig. 8). To the west, the second depocenter is located southwest of the southern fault (segment a in Fig. 8). In this region, the basin infill reaches a maximum thickness of 1.08 km.

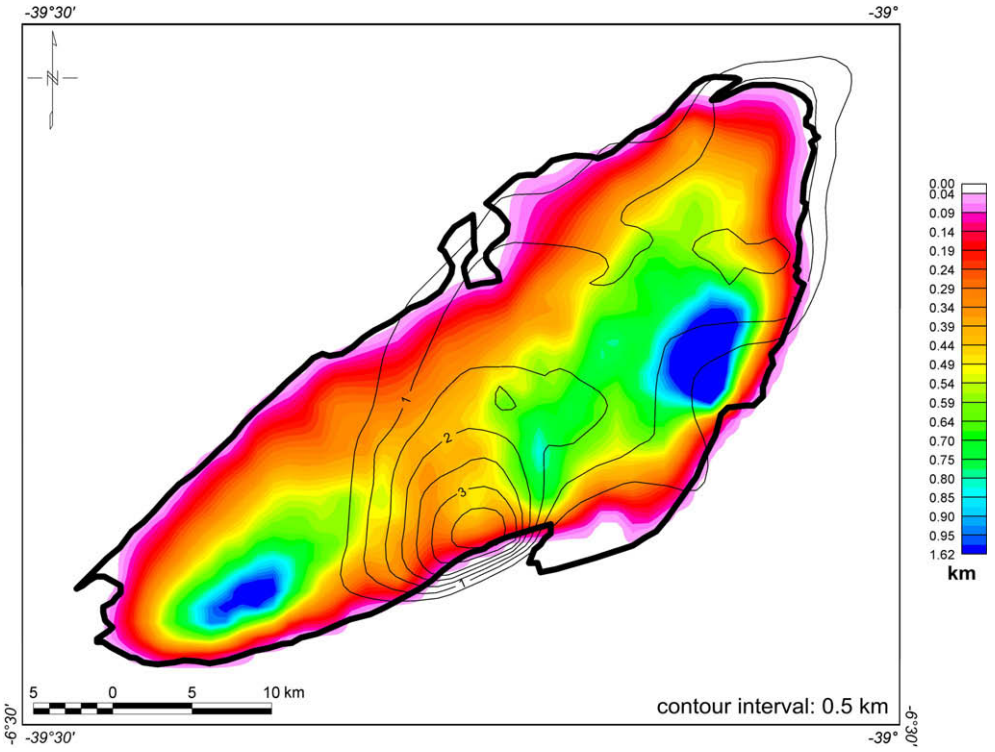

Fig. 7. Composite structural map. Gravity models of the Iguatu basin (colored image), and basement heterogeneity (isopach contour lines in km).

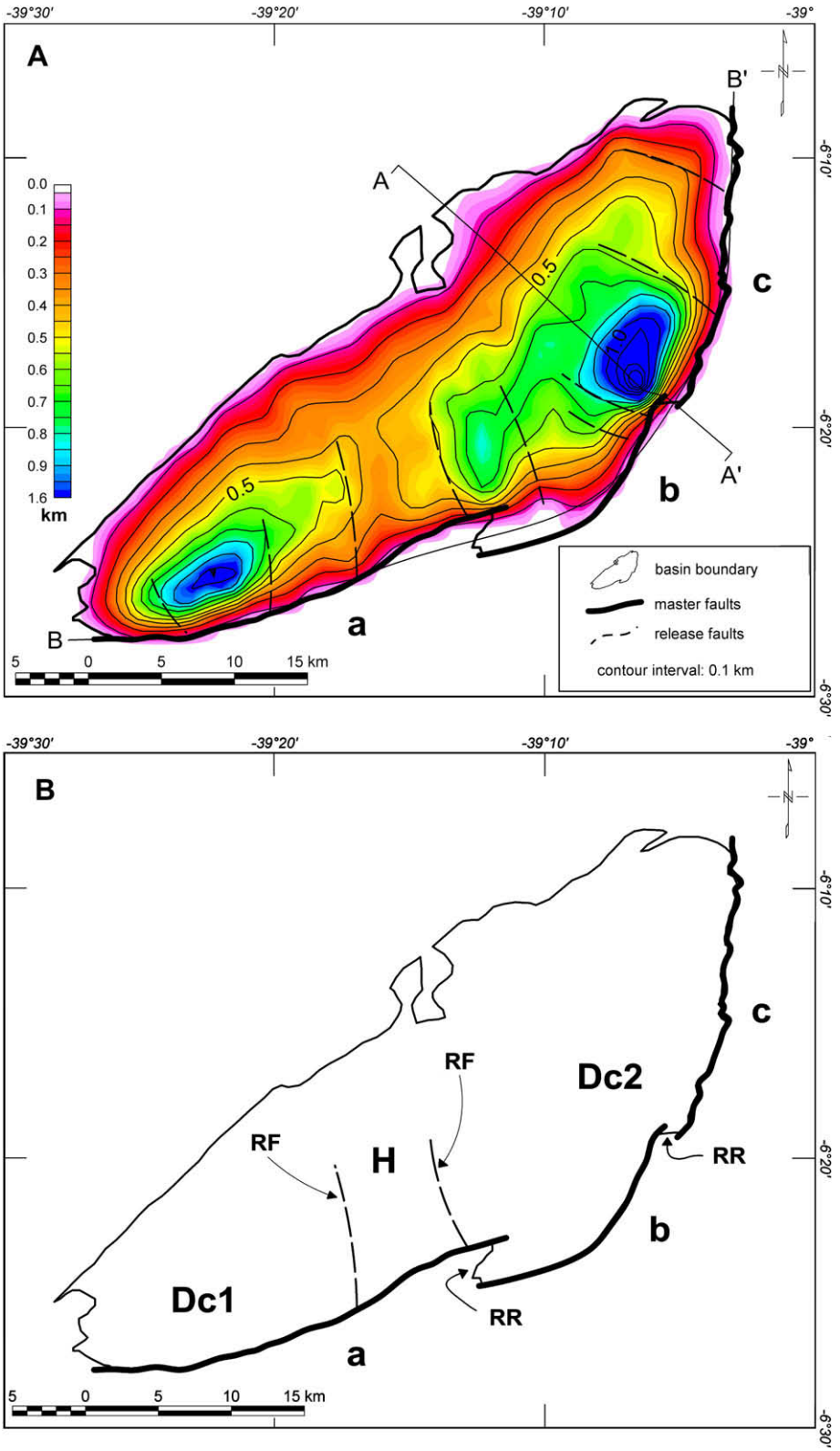

Fig. 8. (A) Basement contour map of the Iguatu basin derived from 3D-gravity modeling with major border fault segments (a, b, and c); and (B) major structural features of the Iguatu basin: depocenters (Dc1 and Dc2), basement high (*H*), relay ramps (RR), and release faults (RF). A–A′ refers to a profile shown in Fig. 10. B–B′ profile is shown in Fig. 11.

In spite of the close similarities in the sedimentary thickness calculation between our study and previous investigations, basin geometry from our gravity modeling differs significantly from previous ones if the heterogeneity of basement rocks is taken into account. Based on gravity modeling, Bedregal (1991) suggested that the Neocomian basin-filling deposits are up to 1.79 km in the deepest depocenter. Even based on a smaller number of gravity stations, that result differs little from the value of 1.62 km obtained in this

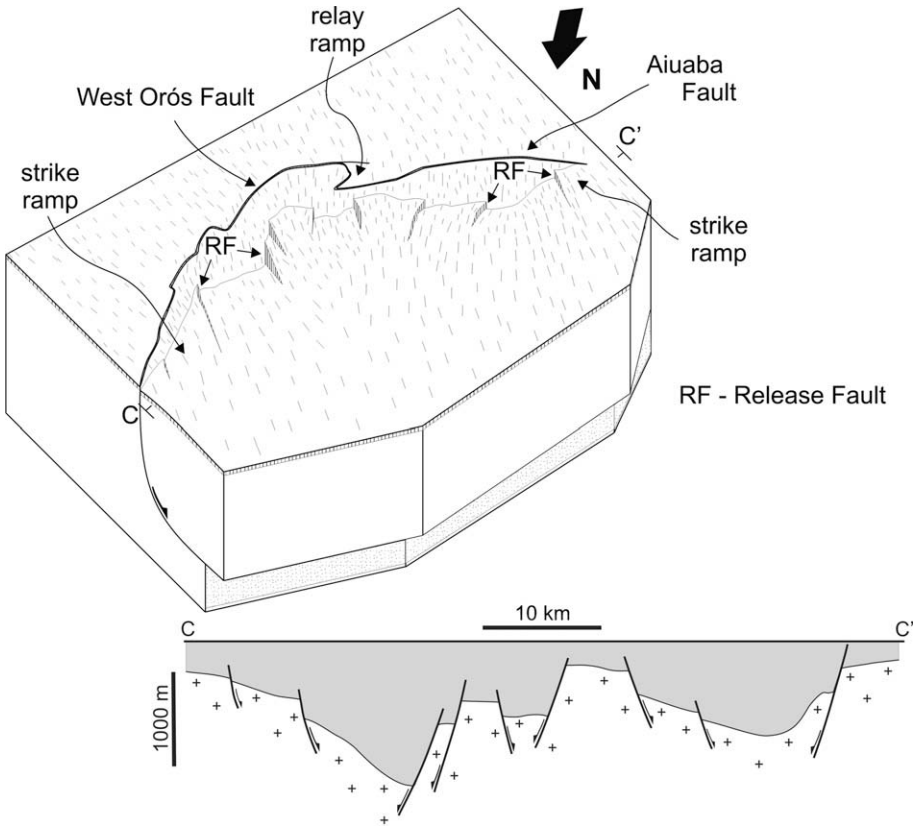

Fig. 9. Block diagram and cross-section showing the internal geometry of the Iguatu basin. Release faults are the cross faults controlling the structural framework of the basin in response to varying throws along the strike of the Aiatuba and West-Orós faults.

study for the maximum basin thickness. In spite of the modeled basin thicknesses having been estimated between 1.6 km and 1.7 km, the rift geometry shown in Fig. 8 differs from the gravity models obtained by Bedregal (1991) and Castro and Castelo Branco (1999). The shallower depocenter (Dc1-SW depocenter) is dislocated southwest in our model in comparison to the previously mentioned models. These differences are probably caused by the interference of the negative anomaly in the center of the basin and the positive anomalies at its western border (see Fig. 6B). A possible explanation is that the previous modeling did not take into account a heterogeneous basement framework, which can interfere in the gravity signature of the basin.

Fig. 10A shows a transect perpendicular to the major depocenter of the Iguatu basin (profile A–A′ in Fig. 8). The radiometric total count is less than 750 cps in the basin, whereas it reaches up to 1500 cps at the graben footwall. We observed low counts in the areas covered by the water of a dam (see Fig. 4). In contrast, the magnetic signature of the basin infill is monotonous, varying from −10 to 10 nT and showing analytic signal low amplitude. Only the master fault is well marked by an outstanding magnetic maximum. Finally, the −15 mGal gravity anomaly represents the internal rift geometry, with a high gradient in the SE faulted border and an incipient gradient in the NW flexural border. Furthermore, Fig. 10A illustrates the rift geometry obtained by the gravity modeling as an asymmetric 1.62 km thick half-graben, representing a unitary rift similar to the half-grabens of the East African Rift System.

5. Fault-segment analysis from the geophysical data

We identified three main fault segments and their geometry (see Figs. 8 and 9). In plan view, fault segments form a right-bend en echelon system. The segments range in length from 18.1 to 32.7 km (a = 32.7 km, b = 18.1 km, and c = 21.8 km), and the fault array is 72.6 km long. The thin line in the fault map indicates possible continuation of the fault segments (see Fig. 8). But because we infer part of fault length, the total length of the segments may be underestimated. Faults exhibit a change in trend from approximately E–W to NE–SW. The three main fault segments curve into the half-graben boundary. The change in fault strike coincides with a similar change in the Precambrian fabric. Synthetic relay ramps occur between the fault segments. In cross-section (see Fig. 9), the faults form structural highs. We constrained a planar geometry of the faults down to the top of the crystalline basement. The major fault segments dip toward north and northwest.

Geophysical data also provide evidence for another type of fault. Gravity lineaments form NW–SE-trending features inside the basin (see Fig. 8). These features occur orthogonal or oblique to the main fault segments. We interpret the features as release faults that form the central horst structure and marginal strike ramps at the basin borders (see Fig. 9). These secondary faults die out within individual hangingwalls and form the rough basement relief beneath the Iguatu basin. The cross-section in Fig. 9B depicts an irregular relief of the basement top, controlled by NW–SE release faults. The release faults we describe in our study were identified elsewhere as faults that accommodate variable displacements along the strike of a normal fault (Destro, 1995).

Knowing the degree to which fault segments interact is important to understanding the faults themselves and the structures associated with them (e.g. Segall and Pollard, 1980). As predicted by most models of fault growth, fault increase leads to an initial fault population of short, low-displacement faults that evolve into a population comprising a few large fault systems (Cowie, 1998; Gupta et al., 1998).

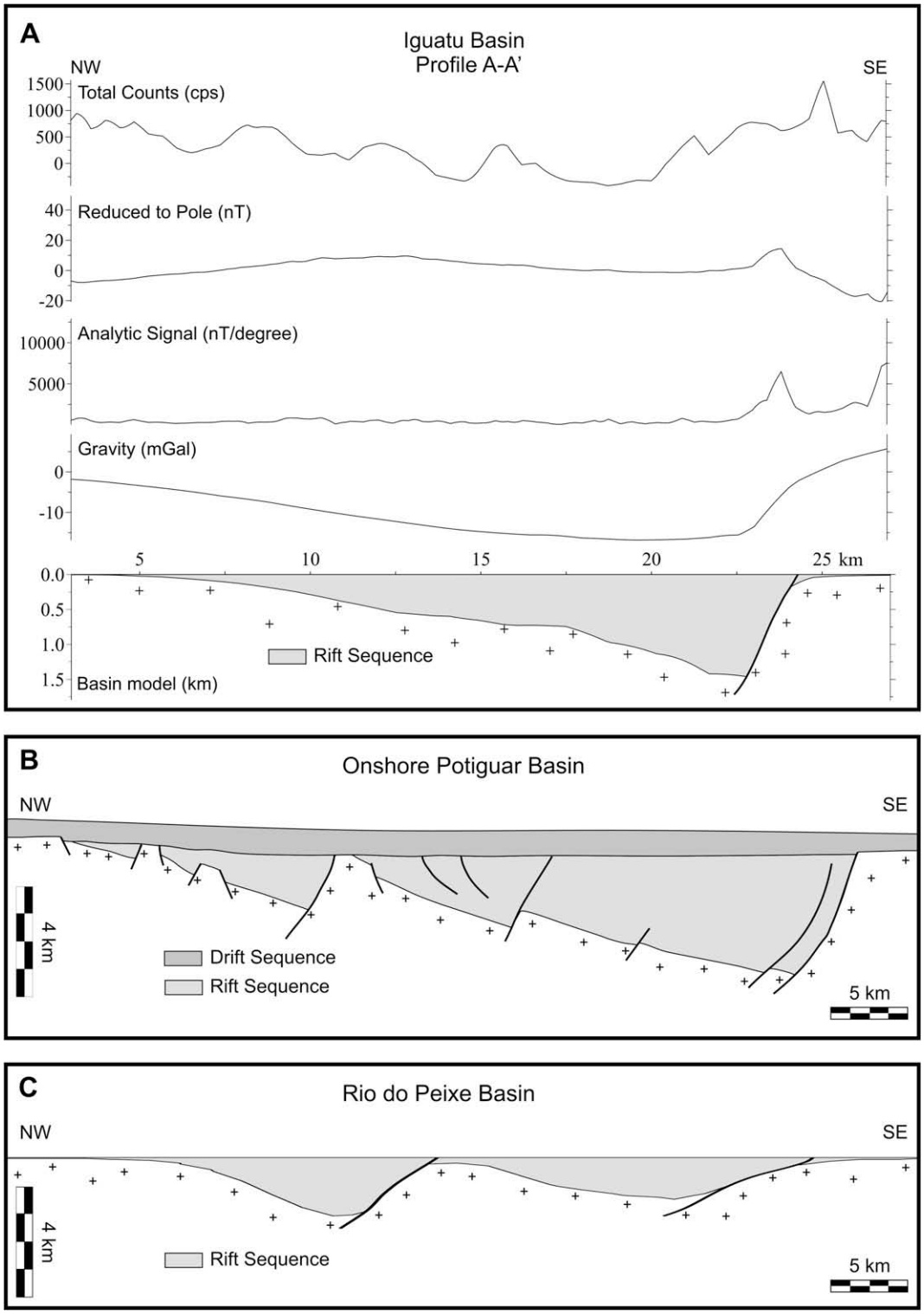

Fig. 10. (A) Geophysical signature of the Iguatu basin along the A–A′ profile; comparison between the rift geometry and geologic sections across (B) the Potiguar basin (Matos, 1992); and (C) Rio do Peixe basin (Castro et al., 2007). See location of A–A′ in Fig. 8.

We analyzed fault growth from a pre-link, multisegment stage fault system. We treated fault segments as single faults in the D/L analysis and we made a few assumptions. We considered that the sediment supply kept pace with the rate of footwall subsidence as a proxy for tectonically controlled accommodation space and fault activity (e.g. Anders and Schlische, 1994; Morley, 2007; Dawers and Underhill, 2000; McLeod et al., 2000). The plot of sediment thickness versus location of measurements in a transect parallel to the fault strike (B–B′ in Fig. 8) indicates the presence, or absence, of isolated depocenters. From such a plot, fault evolution can be inferred (e.g. McLeod et al., 2000). We used a basement contour map of the Iguatu basin derived from 3D-gravity modeling to define fault-segment tips. In addition, the scaling relationship between maximum displacement (D) and maximum trace length

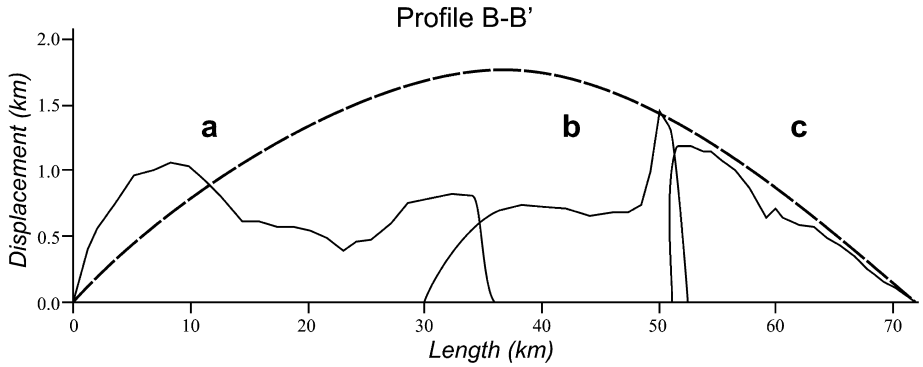

Fig. 11. Displacement profile of fault segments (a, b, and c): broken line represents the profile of an ideal isolated master fault. Profile B–B′ displacement profile runs along the traces of fault segments (a), (b), and (c), as shown in Fig. 8A.

(L) is one of the geometric parameters in the rift internal architecture that can reveal the growth of the master faults and the depocenter formation. Accordingly, we determined throws in successive sections, which are orthogonal to normal–fault strike, by summing the thickness of the sedimentary cover and the height of fault scarp using gravity and Shuttle Radar Topographic Mission (SRTM) data, respectively. We inferred the strike-slip component on the segments to be insignificant. We eventually analyzed fault growth derived from D/L analysis.

We observed the D/L pattern in the central and northern fault segments in the Iguatu basin. We imposed a resolution limit of 17 m for our throw measurements, below which we did not consider any data. The maximum error in sedimentary rock thickness was estimated to be 10%. Using the inverse method described here, Castro et al. (2007) obtained a gravity modeling of the Rio do Peixe basin (Fig. 1), which represents a difference of 7.4% compared with borehole data. We extrapolated this variation to the Iguatu basin and assumed good confidence for the rift architecture. The increase in fault displacement because of fault interaction led to the basin depocenter location. The D/L curve in Fig. 11 is consistent with the interpretation that the southern segment was formed by the linkage of two previously separated minor right-bend en echelon segments.

From the D/L plot, we infer that the fault segments (a, b, and c) propagated toward one another. Fault growth behaved in two different ways: a soft link between the south and central segments and a hard link between the central and northern segments.

The D/L pattern between the central and northern fault segments (segments (b) and (c) in Fig. 11, respectively) indicates high displacement in their northern and southern tips, respectively. The linkage of the two segments increased the rate of displacement in the area where segments overlap. The displacement profile in Fig. 11 illustrates an asymmetric distribution, typical of fault array containing overlapping fault segments with linked relays, as described by Soliva and Benedicto (2004). The D/L curves form steep displacement gradients near their interacting tips at the point of maximum displacement away from the center of both fault segments.

The relationship between the south and central fault segments (segments (a) and (b) in Fig. 8, respectively) indicates two highs on D/L profile, which reveals an independent growth of fault segments during rift initiation. The low displacement between segments (a) and (b) characterizes an intermediary stage in the growth of linked fault segments, named soft linkage stage by Kim and Sanderson (2005). According to them, the soft-linked fault segments grow through the interaction with adjacent faults, which inhibits propagation, and thus they attain high D/L ratios.

The D/L ratios of the three segment faults are 0.040, 0.089, and 0.055, respectively. The maximum D/L ratio of the fault array is 0.024. In the D/L plots of Kim and Sanderson (2005), the D/L ratio of the Iguatu fault array fits the line of normal faults.

The shifting of the point of maximum displacement, d_{max}, toward the interacting tips and the resulting steep and asymmetric displacement gradients indicate fault-segment mechanical interaction. This type of interaction affects fault growth and the final displacement–distance profile of faults (Willemse et al., 1996; Gupta and Scholz, 2000). Therefore, the combined D/L profiles of fault segments mimic that of an isolated fault (e.g., Dawers and Anders, 1995). Our results indicate this kind of evolution and agree with the modeling by Willemse et al. (1996), Willemse (1997), Cowie (1998) and Gupta and Scholz (2000).

The geometry and size of the southern segment suggests that it formed by the link of at least two previously separated minor right-bend en echelon segments. It is possible that the short separation, in comparison with displacement, led to fault-segment linkage on the southern main segment. The previously isolated segments in the south part of the half-graben grew by radial tip propagation, following the growth path $d_{max} = cL^n$, where c is a constant and n is a scaling exponent. A value of 1 is commonly taken for n as a reasonable approximation (Paton, 2006). The continued propagation led to their linkage.

6. Discussion: half-graben evolution

Gravity and airborne radiometric and magnetic data constrained the internal geometry of the Iguatu basin. The resulting geometric models support our hypothesis and previous ones that half-graben evolution represents the coupling of the NW–SE-trending extension and preexisting crustal weaknesses in the Precambrian basement.

The pre-graben heterogeneity comprises the Orós–Jaguaribe domain structural fabric, which is dominated by E–W and NE–SW trending Neoproterozoic shear zones. With subsequent Neocomian extension, the preexisting strike-slip ductile structures were used as seed points for the new extensional faults. With continued extension, the two isolated depocenters coalesced as a 66.5 km long, under-displaced normal fault form (see Figs. 8 and 9).

The half-graben structure was established at the bend of the Aiuaba and West-Orós shear zones (Fig. 2). Rifting started with at least three non-colinear fault segments and two isolated depocenters at the southern and eastern basin boundaries. The basin depocenters migrated with continued extension and growth of the fault segments. Fault segments interacted at relay ramps. Dawers and Underhill (2000) have already observed this pattern in the north-

ern North Sea, where it controlled deposition of Late Jurassic syn-rift deposits.

Our conclusions are in agreement with the study by Bedregal (1991), which was based on structural and gravity analyses. He proposed that a NW–SE extension fuelled fault growth along the preexisting fabric. The accommodation of the resulting strain varied along fault segments. The northern (c) and southern (a) fault segments moved in a transtensional regime, while the central segment (b) moved in an almost pure extension.

Our 3D-gravity modeling incorporates the presence of interfering sources of a heterogeneous crystalline basement and is different from the traditional inversion methods (e.g. Cordell and Henderson, 1968). Therefore, it yielded a more accurate 3D-graben geometry with no influence of neighboring gravity sources. The negative anomaly in Granjeiro domain and in Orós sub-domain, derived from our modeling, could have been generated by a granite body beneath the basin.

Basement highs composed of granite intrusions commonly occur in the northern portion of the Borborema Province favored by extension along ductile shear zones (Almeida et al., 2000; Neves et al., 2000; Castro et al., 2002). Castro et al. (2007) described an example of this kind of basement high, which splits the Rio do Peixe basin into two sub-basins. In that area, the granite intrusion related to the basement high displays a roughly sub-horizontal floor with several gently dipping areas, which they interpreted as magma feeder zones.

The Iguatu basin architecture, represented by an asymmetric half-graben (Fig. 8), is also similar to the internal geometry of Potiguar and Rio do Peixe basins, described by Matos (1992) and Castro et al. (2007), respectively. The cross-sections of these basins (see Fig. 10) suggest that the NW–SE oriented extension affected the NE–SW-trending preexisting weakness zones and formed half-grabens.

We used the observations extracted from the geological and geophysical maps to develop a model for the evolution of the Iguatu fault system that has many similarities to the model proposed by Paton (2006) regarding the South African fault system. Based on seismic data, he described the tectonic evolution of the onshore Gamtoos basin, where two initially separate fault segments with associated isolated depocenters coalesced to form a single depocenter and a master fault. Ponte Filho (1996) also compared the Iguatu basin with the East African Rift System. He pointed out that both rift zones contain a series of half-grabens with similar polarities, which dip to a preferential direction and are separated by basement highs.

7. Conclusions

The purpose of this study was to show new radiometric, magnetic, and gravity data indicating constraint of fault growth and half-graben architecture of the Neocomian Iguatu basin, NE Brazil. This work shows the early stage of propagation of a normal–fault system and examines fault-segment displacement, length, geometry, spacing, overlapping, and relationship with the preexisting basement ductile fabric.

The Iguatu half-graben provides a case study in which both faults and preexisting fabric outcrop and can thus be directly investigated. The radiometric and magnetic signatures of the basement revealed the complexity of the structural framework. In addition, 3D-gravity modeling produced detailed insights about the basin architecture and allowed the identification of the geometry of fault segments.

The NW–SE-trending extension associated with the Pangea breakup deformed continental blocks and generated an elliptic basin anchored in the inflection of the Aiuaba and West-Orós shear zones. These zones reactivated as E–W- and NE–SW-oriented normal faults, respectively. A central horst structure, possibly formed by a granite intrusion, separates the two depocenters.

The crustal anisotropy was determinant in establishing the initiation of the rifting process in the Iguatu basin. This anisotropy controlled the reactivation of shear zones, the evolution of the three normal–fault segments, and the depocenters. Three fault segments occur on the eastern and southern edge of the basin: (a) southern, (b) central, and (c) northern. The three fault segments did not evolve into a system of linked fault segments. They form right-bend en echelon segments that contain a curved geometry and a significant shift in strike. The overlapping fault segments, however, have been linked by relay ramps, where they interact through their stress fields. The relationship between displacement and trace length indicates a separated growth of the fault segments during rift initiation. Overstepped secondary release faults accommodated variable displacements along the strike of master faults and form the central horst structure and marginal strike ramps at the basin borders.

The D/L plot analysis lends support to the existence of several stages of fault growth in the Iguatu basin. Fault segment (a) derived from two minor fault segments, which are now completely linked. Fault segments (b) and (c) present a hard linkage between them. This occurs where fault segments present mechanical interaction and, from the point of view of fault displacement, behave as a single fault. Fault segments (a) and (b) present a soft linkage. This occurs where fault segments interact but still preserve some degree of independence. These various stages of fault segment interaction and linkage are part of the evolution of rift basins. They are observed elsewhere in the region.

Although this study was carried out on a relatively small normal–fault system, the similarities with other rift basins such as the Rio do Peixe and Potiguar basins indicate that the pattern of fault growth we show may be applicable to the normal systems in the region. Our study also indicates that the extension that culminated with the Pangea breakup reactivated in a brittle way the Brasiliano/Pan-African shear zones, preferably in supracrustal terrains intensely deformed and intruded by granite bodies.

Acknowledgments

We thank three anonymous reviewers. They provided careful revision and positive criticism, which greatly improved our work. DLC and FHRB also thank CNPq-Brazil for their PQ grants.

References

Almeida, F.F.M., Brito Neves, B.B., Carneiro, C.D.R., 2000. The origin and evolution of the South American Platform. Earth Science Reviews 50 (1–2), 77–111.

Anders, M.H., Schlische, R.W., 1994. Overlapping faults, intra-basin highs, and the growth of normal faults. Journal of Geology 102, 165–180.

Arthaud, M.H., Vasconcelos, A.M., Nogueira Neto, J.A., Oliveira, F.V.C., Parente, C.V., Monié, P., Liégeois, J.P., Caby, R., Fetter, A., 2000. Main structural features of Precambrian domains from Ceará (NE Brazil). In: Proceedings of the 14th International Conference on Basement Tectonics, Ouro Preto, pp. 84–85.

Bedregal, R.P., 1991. Estudo gravimétrico e estrutural da bacia de Iguatu – CE. M.Sc. Dissertation, UFOP, Ouro Preto, 183p.

Blakely, R.J., 1995. Potential Theory in Gravity and Magnetic Applications. Cambridge University Press, London. 441p.

Blakely, R.J., Jachens, R.C., Calzia, J.P., Langenheim, V.E., 1999. Cenozoic basins of the Death Valley extended terrane as reflected in regional-scale gravity anomalies. Geological Society of America Special Paper, vol. 333, 16p.

Cartwright, J.A., Trudgill, B.D., Mansfield, C.S., 1995. Fault growth by segment linkage: an explanation for scatter in maximum displacement and trace length data from the Canyonlands Grabens of SE Utah. Journal of Structural Geology 17 (9), 1319–1326.

Castro, D.L., 2005. Modelagem gravimétrica 3-D de corpos graníticos e bacias sedimentares com embasamento estrutural de densidade variável. Revista Brasileira de Geofísica 23 (3), 295–308.

Castro, D.L., Castelo Branco, R.M.G., 1999. Caracterização da arquitetura interna das bacias rifte do Vale do Cariri, baseado em modelagem gravimétrica 3-D. Revista Brasileira de Geofísica 17 (2–3), 129–144.

Castro, D.L., Medeiros, W.E., Jardim de Sá, E.F., Moreira, J.A.M., 1998. Mapa gravimétrico do Nordeste Setentrional do Brasil e margem continental adjacente: interpretação com base na hipótese de isostasia. Revista Brasileira de Geofísica 16 (2/3), 115–131.

Castro, D.L., Castelo Branco, R.M.G., Martins, G., Castro, N.A., 2002. Radiometric, magnetic, and gravity study of the Quixadá Batholith, Central Ceará Domain (NE-Brazil): evidence for an extension controlled emplacement related to the Pan-African/Brasiliano collage. Journal of South American Earth Sciences 15 (5), 543–551.

Castro, D.L., Oliveira, D.C., Castelo Branco, R.M.G., 2007. On the Tectonics of the Neocomian Rio do Peixe rift basin, NE Brazil: lessons from gravity, magnetics and radiometric data. Journal of South American Earth Sciences 24 (2–4), 186–202.

Cavalcante, J.C., 1999. Limites e evolução geodinâmica do sistema Jaguaribeano, Província Borborema, NE Brasil. M.Sc. Dissertation, UFRN, Natal, 183p.

Cordell, L., Henderson, R.G., 1968. Iterative three dimensional solution of gravity anomaly used a digital computer. Geophysics 33, 596–601.

Cordell, L., Phillips, J.D., Godson, R.H., 1992. US Geological Survey Potential Field geophysical software Version 2.0, USGS, Open File Report 92-18.

Cowie, P.A., 1998. Normal fault growth in three-dimensions in continental and oceanic crust. In: Buck, R., Delaney, P., Karson, J., Lagabrielle, Y. (Eds.), Faulting and Magmatism at Mid-Ocean Ridges, AGU Monograph, 106p.

Cowie, P.A., Gupta, S., Dawers, N.H., 2000. Implications of fault array evolution for synrift depocentre development: insights from a numerical fault growth model. Basin Research 12, 241–261.

Dawers, N.H., Anders, M.H., 1995. Displacement-length scaling and fault linkage. Journal of Structural Geology 17, 607–614.

Dawers, N.H., Underhill, J.R., 2000. The role of fault interaction and linkage in controlling syn-rift stratigraphic sequences: Late Jurassic, Statfjord East area, northern North Sea. American Association of Petroleum Geologists Bulletin 84, 45–64.

Dawers, N.H., Anders, M.H., Scholz, C.H., 1993. Fault length and displacement: scaling laws. Geology 21, 1107–1110.

Destro, N., 1995. Release fault: a variety of cross fault in linked extensional fault systems, in the Sergipe-Alagoas basin, NE Brazil. Journal of Structural Geology 17 (5), 615–629.

Gomes, J.R.C., 1981. Projeto Radambrasil, cartas 24-25, Jaguaribe and Natal. Geologia, Geomorfologia, Pedologia, Vegetação e Uso Potencial do solo. MME, Rio de Janeiro, pp. 27–300.

Gupta, A., Scholz, C.H., 2000. A model of normal fault interaction based on observations and theory. Journal of Structural Geology 22, 865–879.

Gupta, A., Cowie, P.A., Dawers, N.H., Underhill, J.R., 1998. A mechanism to explain rift-basin subsidence and stratigraphic patterns through fault-array evolution. Geology 26, 595–598.

Jachens, R.C., Moring, B.C., 1990. Maps of thickness of Cenozoic deposits and the isostatic residual gravity over basement for Nevada. US Geological Survey Open-File Report 90-404, scale 1:1,000,000.

Kim, Y.-S., Sanderson, D.J., 2005. The relationship between displacement and length of faults: a review. Earth Science Reviews 68, 317–334.

Matos, R.M.D., 1992. The northeast Brazilian rift system. Tectonics 11 (4), 766–791.

McLeod, A.E., Dawers, N.H., Underhill, J.R., 2000. The propagation and linkage of normal faults: insights from Strathspey-Brent-Statfjord fault array, northern North Sea. Basin Research 12, 263–284.

Mello, U.T., 1989. Controles tectônicos na estratigrafia da Bacia Potiguar: uma integração de modelos geodinâmicos. Boletim de Geociências da Petrobrás 3 (4), 347–364.

MME/CPRM, 1995. Catálogo Geral de Produtos e Serviços, Geologia, Levantamentos Aerogeofísicos – Database AERO. Rio de Janeiro, 359p.

Morley, C.K., 2007. Variations in late Cenozoic-recent strike-slip and oblique-extensional geometries, within Indochina: the influence of pre-existing fabric. Journal of Structural Geology 29, 36–58.

Nabighian, M.N., 1984. Towards a three-dimensional automatic interpretation of potential field data via generalized Hilbert transforms: fundamental relations. Geophysics 49, 780–786.

Neves, S.P., Vauchez, A., Feraud, G., 2000. Tectono-thermal evolution, magma emplacement, and shear zone development in the Caruaru area (Borborema Province, NE Brazil). Precambrian Research 99, 1–32.

Oliveira, D.C., Chang, H.K., 1993. Petrogênese do magmatismo Rio Ceará Mirim (NE do Brasil): um exemplo do uso de enxame de diques no estudo dos processos termo-mecânicos da Litosfera. In: Proceedings of the 3rd International Congress of the Brazilian Geophysical Society, Expanded Abstract, vol. 2, pp. 1122–1127.

Paton, D.A., 2006. Influence of crustal heterogeneity on normal fault dimensions and evolution: southern South Africa extensional system. Journal of Structural Geology 28, 868–886.

Peacock, D.C.P., 2002. Propagation, interaction and linkage in normal fault systems. Earth Science Reviews 58, 121–142.

Pickering, G., Peacock, D.C.P., Sanderson, D.J., Bull, J.M., 1997. Modelling tip zones to predict the displacement and length characteristics of faults. American Association of Petroleum Geologists Bulletin 81, 82–99.

Ponte Filho, F.C., 1996. Análise estratigráfica e estrutural das bacias de Iguatu, Estado do Ceará. MsC. Dissertation, UNESP, Rio Claro, 192p.

Rao, D.B., Babu, N.R., 1991. A Fortran-77 computer program for three-dimensional analysis of gravity anomalies with variable density contrast. Computers and Geosciences 17 (5), 655–667.

Sá, J.M., McReath, I., Leterrier, J., 1995. Petrology, geochemistry and geodynamic setting of Proterozoic igneous suites of the Orós fold belt (Borborema Province, Northeast Brazil). Journal of South American Earth Science 8 (3/4), 299–314.

Segall, P., Pollard, D.D., 1980. Mechanics of discontinuous faults. Journal of Geophysical Research 85, 4337–4350.

Soliva, R., Benedicto, A., 2004. A linkage criterion for segmented normal faults. Journal of Structural Geology 26, 2251–2267.

Telford, W.M., Geldart, L.P., Sheriff, R.E., Keys, D.A., 1998. Applied Geophysics, fifth ed. Cambridge University Press. 860p.

Vasconcelos, A.M., Gomes, F.E.M., 1998. Programa Levantamentos Geológicos Básicos do Brasil – PLGB. Iguatu – Folha SB.24-Y-B, Estado do Ceará, CPRM/DIEDIG/DEPAT, Brasília, 107p.

Willemse, E.J.M., 1997. Segmented normal faults: correspondence between three dimensional mechanical models and field data. Journal of Geophysical Research 102 (B1), 675–692.

Willemse, E.J.M., Pollard, D.D., Aydin, A., 1996. 3-Dimension analysis of slip distributions on normal–fault arrays with consequence for fault scaling. Journal of Structural Geology 18, 295–309.